Three Putative Types of El Niño Revealed by Spatial Variability in Impact on Australian Wheat Yield

A. B. POTGIETER

Department of Primary Industries, Toowoomba, Queensland, Australia

G. L. HAMMER

Department of Primary Industries, Toowoomba, and School of Land and Food Sciences, The University of Queensland, Brisbane, Queensland, Australia

H. MEINKE AND R. C. STONE

Department of Primary Industries, Toowoomba, Queensland, Australia

L. GODDARD

International Research Institute for Climate Prediction, Lamont-Doherty Earth Observatory, Columbia University, Palisades, New York

(Manuscript received 29 September 2003, in final form 13 October 2004)

ABSTRACT

The El Niño–Southern Oscillation (ENSO) phenomenon significantly impacts rainfall and ensuing crop yields in many parts of the world. In Australia, El Niño events are often associated with severe drought conditions. However, El Niño events differ spatially and temporally in their manifestations and impacts, reducing the relevance of ENSO-based seasonal forecasts. In this analysis, three putative types of El Niño are identified among the 24 occurrences since the beginning of the twentieth century. The three types are based on coherent spatial patterns ("footprints") found in the El Niño impact on Australian wheat yield. This bioindicator reveals aligned spatial patterns in rainfall anomalies, indicating linkage to atmospheric drivers. Analysis of the associated ocean–atmosphere dynamics identifies three types of El Niño differing in the timing of onset and location of major ocean temperature and atmospheric pressure anomalies. Potential causal mechanisms associated with these differences in anomaly patterns need to be investigated further using the increasing capabilities of general circulation models. Any improved predictability would be extremely valuable in forecasting effects of individual El Niño events on agricultural systems.

1. Introduction

The El Niño–Southern Oscillation (ENSO) is a dynamic ocean–atmosphere phenomenon with a genesis region in the tropical Pacific (Cane 2000). It affects rainfall and crop yield in many parts of the world (Ropelewski and Halpert 1987; Garnett and Khandekar 1992). Understanding of ENSO has provided some predictability for ensuing seasonal rainfall (Stone et al. 1996) and crop yield (Nicholls 1985). The extreme warm phase of ENSO (i.e., El Niño) recurs approximately every 2–7 yr and is often associated with severe droughts in Australia and elsewhere (Allan 2000). Various studies have investigated the relationship between ENSO and Australian rainfall and found it to be significant particularly in eastern parts of Australia (Pittock 1975; Ropelewski and Halpert 1987; McBride and Nicholls 1983; Stone et al. 1996; Mason and Goddard 2001). However, although the phases of ENSO are often classified as either El Niño (EN), La Niña (LN), or neutral (NT), individual EN or LN events are never exactly the same, either in terms of ocean–atmosphere anomalies or their consequences on rainfall and ecosystems. They vary at a spatiotemporal scale in terms of their intensity, spatial extent, onset, duration, and cessation (Allan et al. 1996).

Rainfall variability is the dominant factor causing year-to-year fluctuations in Australian wheat yield (Nix 1975). Previous research has examined the relation-

Corresponding author address: Andries Potgieter, Department of Primary Industries, P.O. Box 102, Toowoomba, QLD 4350 Australia.
E-mail: andries.potgieter@dpi.qld.gov.au

ships among rainfall variability, indicators of ENSO, and observed Australian wheat yields and found them to be significant at a national scale (Rimmington and Nicholls 1993; Hill et al. 2001; Potgieter et al. 2002). Crop simulation models can be used to assess the overall effect of the interactions between climate and other factors contributing to yield variability (e.g., soil type and cultivar). They have been successfully applied to generate long time sequences of wheat yields to quantify the impact of rainfall variability on production risk at farm (Nelson et al. 2002) or at regional scale (Stephens and Lyons 1998; Stephens et al. 2000). We have shown previously, using the full time series generated from a regional modeling approach (Potgieter et al. 2002), that indicators of ENSO (Stone et al. 1996) significantly affect wheat yield throughout the major production zones in the Australian wheat belt. However, the relationship is not temporally coherent across the zones. While in aggregate the relationship for each zone is similar (e.g., on average the EN phase is associated with reduced yield in all zones), the effects differ across zones in any particular year.

ENSO-related droughts not only severely impact regional ecosystems, farm income, and enterprise viability, they also affect macroeconomic indicators such as employment and economic growth (White 2000). Severe drought can cause reduction in Australia's Gross National Product of up to 2% (Anderson 1979; Hogan et al. 1995). In September 2002 (an EN year), the economic growth for 2002/2003 was reduced by 0.5% points, which reflected flow-on effects from the adverse effect of drought in rural Australia (ABARE 2002).

The objective of this study was to examine the spatial variability of wheat yields within EN years and assess likely global climate drivers associated with any coherent patterns of variability across the Australian wheat belt. Although prediction of EN years has improved considerably over the last decade, the features of EN events that generate this spatial variability in impact on ecosystems (i.e., wheat yield) remains to be elucidated. Here, we investigate the extent and intensity of wheat yield anomalies during the extreme warm phase of ENSO and consider the broad ocean–atmosphere dynamics related to the wheat yield anomaly patterns.

2. Methods

a. Simulated shire wheat yields

To identify spatial patterns in Australian wheat yield, we used a simple agro-climatic model (Stephens 1998) to simulate shire wheat yield for each year from the beginning of the twentieth century for each of the 284 main wheat-producing shires in Australia. The model was trained on 19 yr of recent (1975–93) shire production and rainfall records and explained 90% of the temporal variation in yield at the national scale. The model reproduced spatial patterns of shire yield with a spatial correlation averaging 0.86 over the training period (Potgieter et al. 2002). By applying this model using historical rainfall data for the period 1900–2002, we generated a time series of yield data that reflects realistically what the wheat crop throughout the Australian wheat belt would have yielded given current technology (i.e., 2002) and production distribution for any season experienced since the beginning of the twentieth century.

b. El Niño occurrences

The EN events in the period 1901–2002 were derived from a classification system based on the combination of ocean and atmospheric datasets. The extended reconstructed SST (ERSST; Smith and Reynolds 2003) and Troup Southern Oscillation index (SOI; Troup 1965) datasets were used. Using the SST time series for Niño-3.4, a year was classified as EN if the 5-month running mean was greater than or equal to 0.5 for 6 or more months between April and December (Trenberth 1997). Using the SOI time series, a year was classified as EN if the 3-month running mean was less than or equal to –5.5 for 6 or more months between April and December (Ropelewski and Jones 1987). The period April–December is concurrent with the wheat-growing season and almost always encompasses the start (i.e., April–May) and peak (October–December) of an EN event. The threshold value for the classification of EN years based solely on SST for Niño-3.4 or based solely on SOI yielded near 25% occurrence in either case. Accepting either criterion resulted in 24 EN years in the 102 yr used in this analysis (Table 1).

c. Principal component analysis and clustering of wheat yields

Principal component analysis was performed on the wheat yield data matrix (284 shires $\times$ 24 EN years) to identify the significant orthogonal factors that retained the spatial variability among years. Factors were retained if associated eigen values were greater than one (Kaiser 1958). Cluster analysis was conducted on the factor loadings for each EN year to form objectively defined year groups. Clustering was performed using an agglomerative hierarchical approach and Ward's minimum variance linking method (Gong and Richman 1995) with Euclidean distance as the similarity measure (Mimmack et al. 2001).

d. Rainfall anomaly maps

Rainfall variability is the predominate cause of shire wheat yield variability in Australia (Potgieter et al. 2002). Wheat yield represents the integrated consequence of variation in amount, frequency, timing, and intensity of rainfall events over long periods. This integrative quality makes the simulated wheat yield footprints an ideal diagnostic tool for identifying

TABLE 1. The 24 EN years identified when the criterion based on either SOI or SST in Niño-3.4 was accepted.

Year	SOI	SST	Year	SOI	SST	Year	SOI	SST
1901			1935			1969		✓
1902		✓	1936			1970		
1903			1937			1971		
1904			1938			1972	✓	✓
1905	✓	✓	1939			1973		
1906			1940	✓	✓	1974		
1907			1941	✓	✓	1975		
1908			1942			1976		
1909			1943			1977	✓	✓
1910			1944			1978		
1911	✓		1945			1979		
1912			1946	✓		1980		
1913			1947			1981		
1914	✓		1948			1982	✓	✓
1915			1949			1983		
1916			1950			1984		
1917			1951	✓		1985		
1918			1952			1986		
1919	✓		1953	✓	✓	1987	✓	✓
1920			1954			1988		
1921			1955			1989		
1922			1956			1990		
1923			1957		✓	1991	✓	✓
1924			1958			1992	✓	✓
1925	✓		1959			1993	✓	✓
1926			1960			1994	✓	✓
1927			1961			1995		
1928			1962			1996		
1929			1963			1997	✓	✓
1930			1964			1998		
1931			1965	✓	✓	1999		
1932			1966			2000		
1933			1967			2001		
1934			1968			2002	✓	✓

broadly based seasonal to annual climatic drivers. Rainfall anomaly patterns were generated and mapped for growing-season (May–October) rainfall across the Australian wheat belt. Average anomalies from the associated climatological mean were determined for the groups of years defined in the cluster analysis of the wheat yield data. Maps of the weighted standardized shire rainfall anomalies were created for each footprint. This enabled inspection of alignment of rainfall during this period (i.e., May–October) with the wheat footprints and consequently with the associated climate dynamics during the associated footprint years. It should be noted that this approach is contrary to traditional climatic analyses that investigate climatic drivers first, then attempt to identify similarities of rainfall patterns, and finally try to link such similarities to agricultural impacts.

e. Global SST and MSLP anomaly maps

Composite maps of the ERSST (1901–2002) and MSLP (1901–94) anomalies were created for 3-monthly intervals before [January–February–March (JFM; hereafter, 3-month periods are denoted by the first letter of each respective month)] and during (AMJ, JAS, and OND) the wheat-growing season. Average anomalies from the associated climatological mean were determined for groups of years defined in the cluster analysis in a similar manner to that for the rainfall anomalies. Contours were shaded if consistency of anomalies among years within each cluster group reached significance at the 90% level (Mason and Goddard 2001).

3. Results and discussion

a. Wheat yield footprints in El Niño years

Spatial variations in EN impact on wheat yield were analyzed across the 284 shires by isolating the data for the 24 EN events in the 102-yr time series. Principal component analysis extracted two distinct patterns that accounted for 89% of the total variation among the 24 yr. Cluster analysis of the rotated principal component loadings identified four possible groups of years among the EN years. However, as one of these four groups had only two members, the level of clustering yielding three groups was adopted to ensure adequate representation in each group for subsequent analysis (Fig. 1).

We mapped the average standardized shire wheat yield anomaly for each cluster of years to derive the associated spatial pattern of impact on wheat yield. These yield impact patterns or El Niño "footprints" differ in their extent and magnitude, providing a sound bioindicator of EN impact for each group (Fig. 2). Footprint 1 (FP1; Fig. 2a), which contains 9 yr in group 1 (Fig. 1), has below average shire wheat yield in Queensland (QLD), while the remainder of the wheat belt experiences average [Western Australia (WA)] to above average [parts of Victoria (VIC) and New South Wales (NSW)] shire wheat yield. Footprint 2 (FP2;

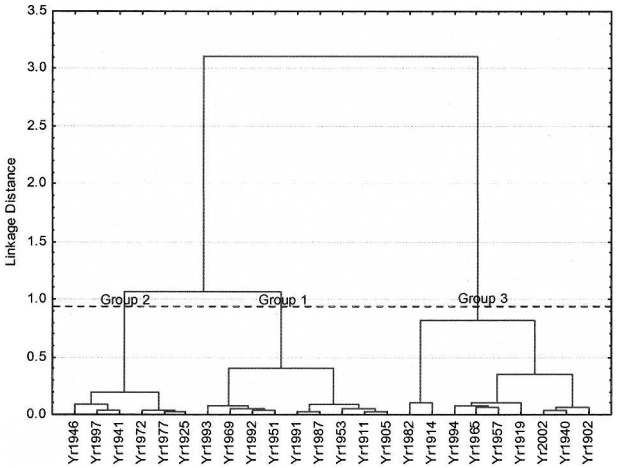

FIG. 1. Clustering of the 24 El Niño years based on their factor loadings from the principle component analysis. The dotted line indicates the cutoff used to form the three groups. Group 1 contains 9 yr, group 2 has 6 yr, and group 3 has 9 yr.

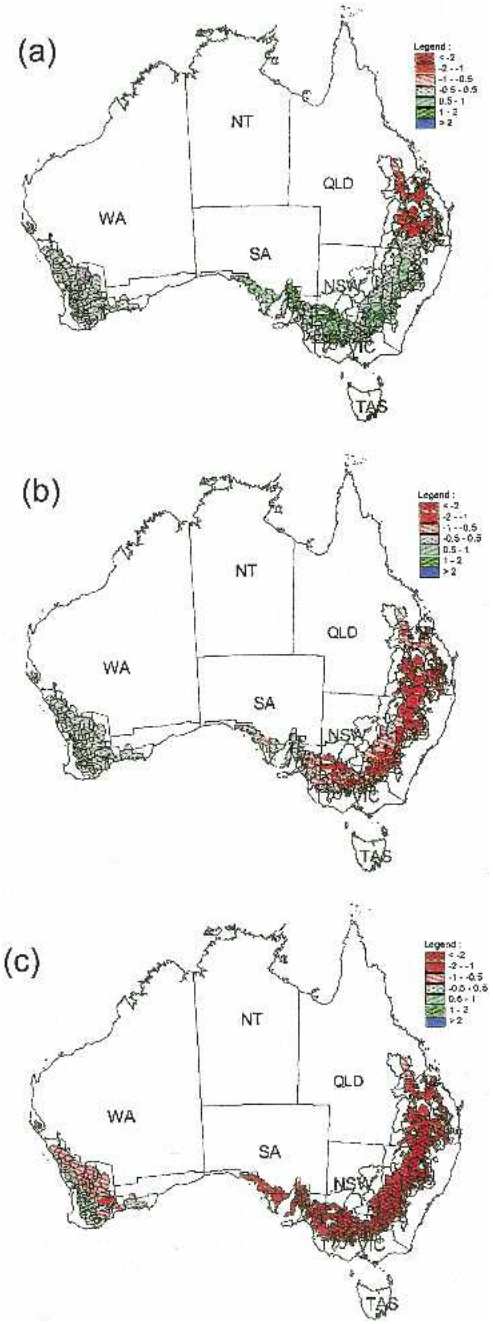

FIG. 2. Average standardized (relative to all years) shire wheat yield anomalies or impact FPs during EN years for (a) cluster-1 EN years (FP1), (b) cluster-2 EN years (FP2), and (c) cluster-3 EN years (FP3). Categories represent number of standard deviations of the average anomaly from the long-term mean.

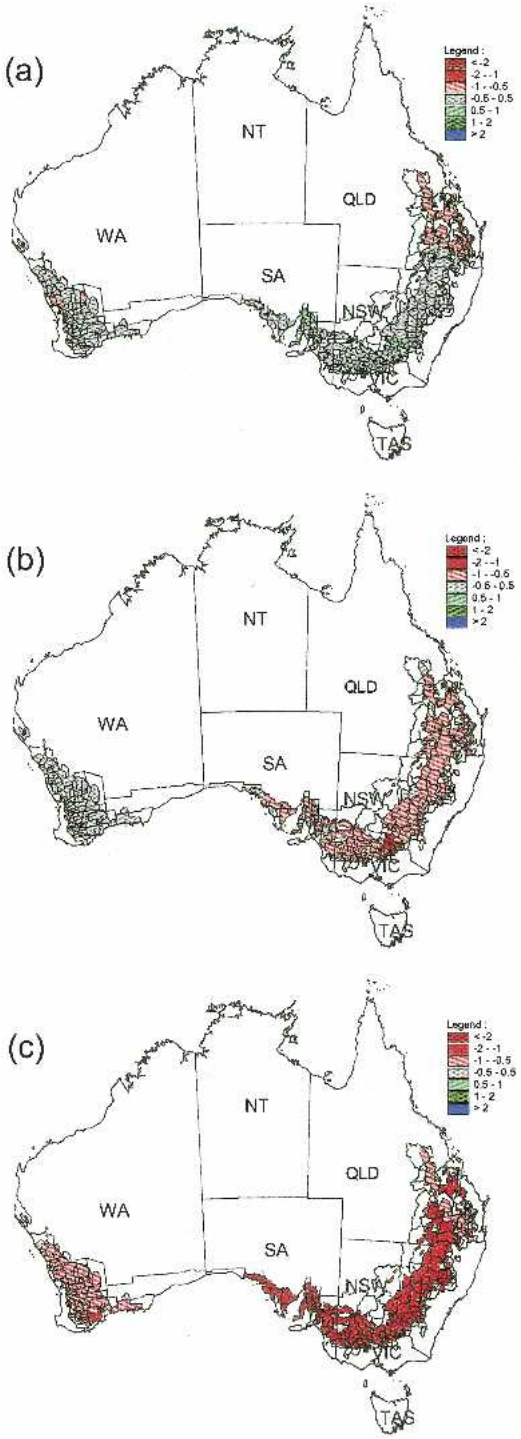

FIG. 3. Weighted standardized (relative to all years) shire rainfall anomalies for May–Oct rainfall during EN years associated with (a) FP1, (b) FP2, and (c) FP3. Categories represent number of standard deviations of the average anomaly from the long-term mean.

Fig. 2b) consists of 6 yr in group 2 with below-average shire wheat yield in most of southern and eastern Australia, while shires in WA experience near-average yield. For the 9 yr in group 3, which form footprint 3 (FP3), nearly the whole of the Australian wheat belt experienced below-average yield, and anomalies were severe in many areas. These years were associated with devastating consequences for the entire Australian wheat industry. It is noteworthy that only the QLD region is affected negatively in all three cases.

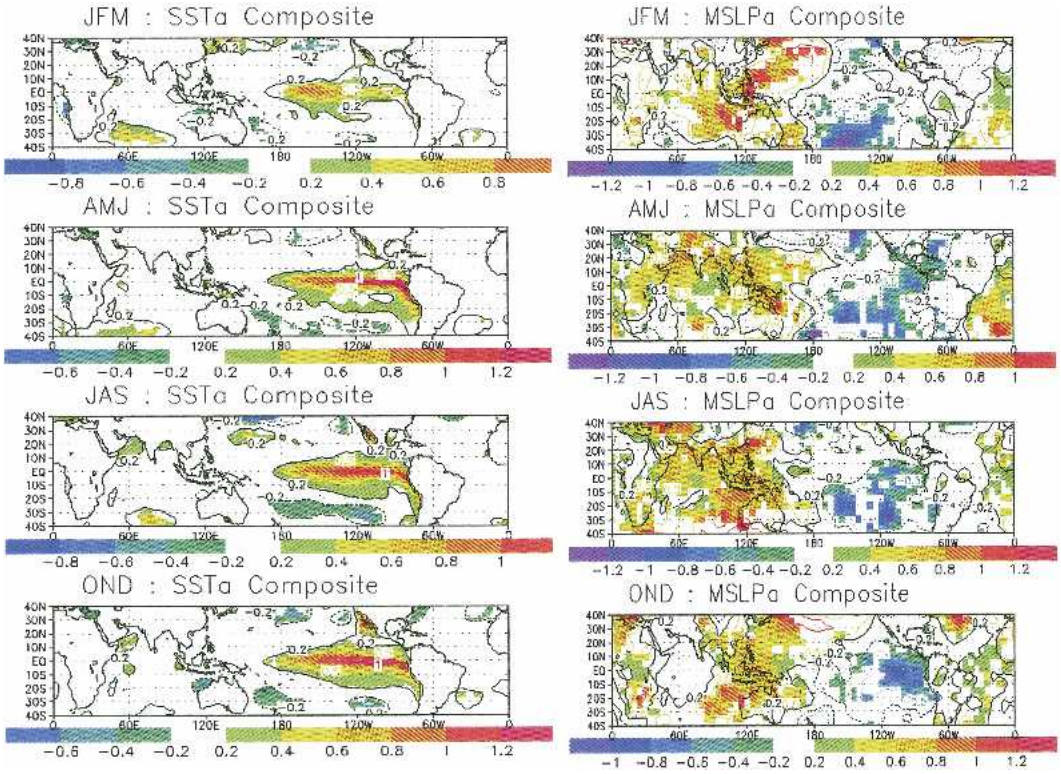

FIG. 4. Composite maps of 3-month-averaged (left) SST anomalies and (right) MSLP anomalies for the years in each EN impact FP: years in (a) FP1, (b) FP2, and (c) FP3 for seasons JFM to OND. Shaded areas indicate where the anomalies of the composite members share the same sign as the composite in a statistically significant (90% level) number of cases relative to the sample size. This level of significance is reached if 7 of 9 yr match the sign of the composite for FP1 and FP3 SST composites, and 5 of 6 yr for FP2 SST composites. The requirement for the MSLP composites is 7 of 9 yr for FP1, 5 of 5 yr for FP2, and 7 of 8 yr for FP3.

b. Rainfall anomaly patterns associated with wheat yield footprints

The May–October rainfall anomaly patterns were mapped for the same three clusters of years used in deriving the wheat yield footprints. May–October represents the main growing season for wheat across the Australian wheat belt. The patterns in rainfall anomalies (Fig. 3) aligned closely with those for wheat yield in the three FPs (Fig. 2). Below-average rainfall anomalies were evident in QLD for years in FP1 (Fig. 3a), whereas they occurred throughout southern and eastern Australia for years in FP2 (Fig. 3b). For years in FP3, rainfall anomalies were more severe and spread across the entire wheat belt (Fig. 3c). The significant spatial coherence of the shire wheat yields and weighted rainfall anomalies for each FP year group suggests a strong connection to atmospheric drivers that generate relatively persistent weather patterns. This result also demonstrates the value of using an integrating biological system, like a wheat crop, to identify coherent patterns in climatic influences that might not have otherwise been uncovered. Attempts to generate distinct FPs from the May–October rainfall period yielded six or more likely groups (data not shown) rather than the three groups resulted from the wheat model. This could indicate a greater degree of complexity in rainfall data versus the integrated effect of rainfall as measured by the wheat model (Meinke et al. 2003).

c. Connecting wheat yield footprints with global SST and MSLP patterns

To investigate connections between yield impact footprints and climate drivers, we examined dynamics of spatial patterns in average global SST and mean sea level pressure (MSLP) anomalies for the years associated with each FP. As expected, SST and MSLP anomaly composites of all three FP year groups evolved into the classical EN pattern with warmer than normal water in the equatorial Pacific Ocean developing by midyear along with the associated pressure anomaly dipole between eastern [low pressure (LP)] and western [high pressure (HP)] Pacific zones (Fig. 4). However, there were differences in timing of onset, extent, and location of the anomalies among the three groups.

Composite anomaly patterns for years in FP1 showed slightly warmer than normal SSTs in the equatorial Pacific by the end of March (Fig. 4a). During AMJ and JAS, the warm SSTs in the Tropics intensified in the

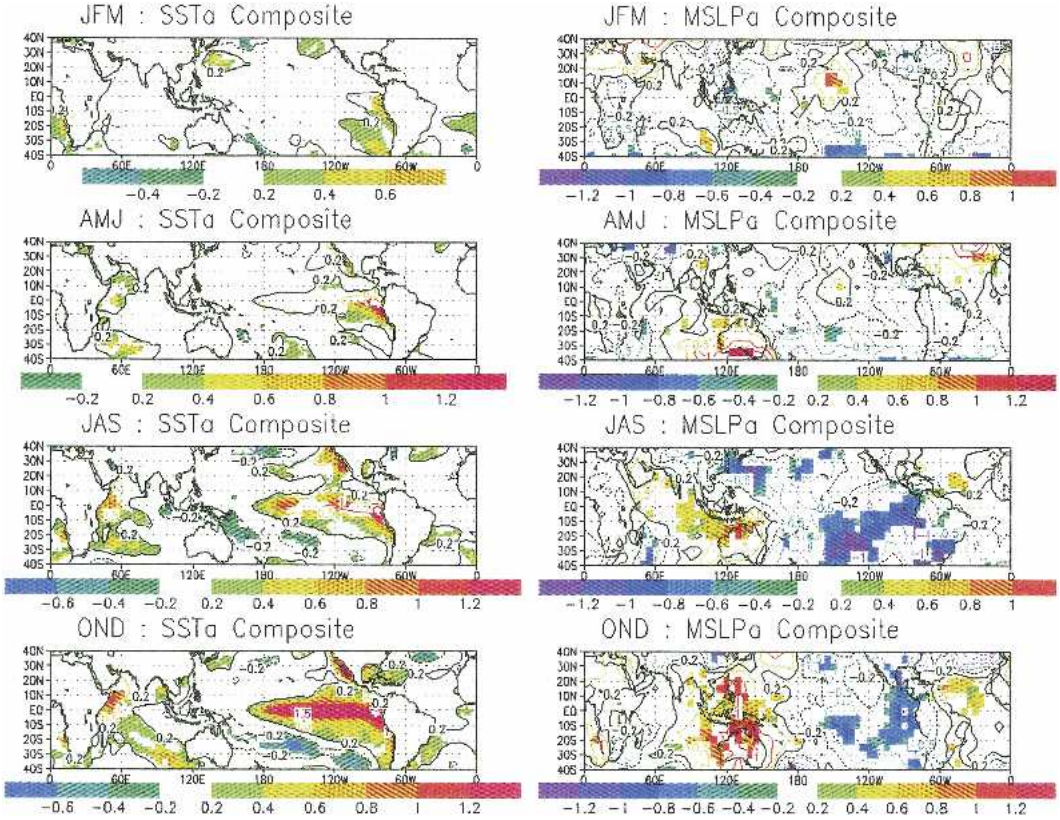

FIG. 4. (*Continued*)

central to eastern tropical Pacific region with very much above average SSTs farther east closer to the South American coast. At the same time, a pool of anomalously cool water developed in the southern Pacific. Significant HP anomalies developed in JFM over Indonesia and extended over northeastern Australia by AMJ. These HP anomalies remained over Indonesia and northern Australia during the second half of the growing season (JAS and OND; Fig. 4a). This coincided with LP anomalies that formed in the central southern Pacific during JFM but were focused over the eastern tropical Pacific during the remainder of the year. The HP anomalies over northern Australia and LP anomalies over the Pacific Ocean create the well-known dipole pressure pattern, which is the basis of the Southern Oscillation index that has been used widely as an indicator of phases of the ENSO phenomenon (Troup 1965). The centers of activity of the opposing components of the dipole were located near the equator and were widely separated for this group of years.

HP anomalies are usually associated with reduced rainfall likelihood in their area of influence. The persistence of HP anomalies over much of the far north of the continent may explain the very much below average shire wheat yields in QLD for years in FP1. The associated anticyclonic cells (HP systems) exert an influence across large areas of the north, bringing hot, dry stable conditions. However, this also allows the inflow of cool and moist air masses across southern Australia (Nix 1975). This may explain the lack of effect on wheat yield in other parts of Australia during EN years in FP1.

For years in FP2, consistently warmer than normal SSTs were not evident until JAS (Fig. 4b), but high-magnitude anomalies were more widespread than for years in FP1, especially in the central tropical Pacific late in the season (OND). In addition, a pool of anomalously cool water developed near the east coast of Australia in JAS. At the same time, significant warm anomalies developed in the western Indian Ocean and propagated toward the WA coast during OND. Concurrent MSLP anomalies (Fig. 4b) were not fully consistent among years but indicated a more proximal pressure dipole than in FP1, with LP anomalies in the central Pacific (more to the southwest than for FP1) and HP anomalies centered more to the southeast, especially late in the season (OND). This difference likely explains extension of the impact zone to all of eastern Australia for years in FP2. SST anomalies in the Indian Ocean may have moderated effects in southwestern Australia.

For years in FP3, warmer than normal SST anomalies appeared early (Fig. 4c), as for years in FP1, but the anomalies intensified more near the date line and in the

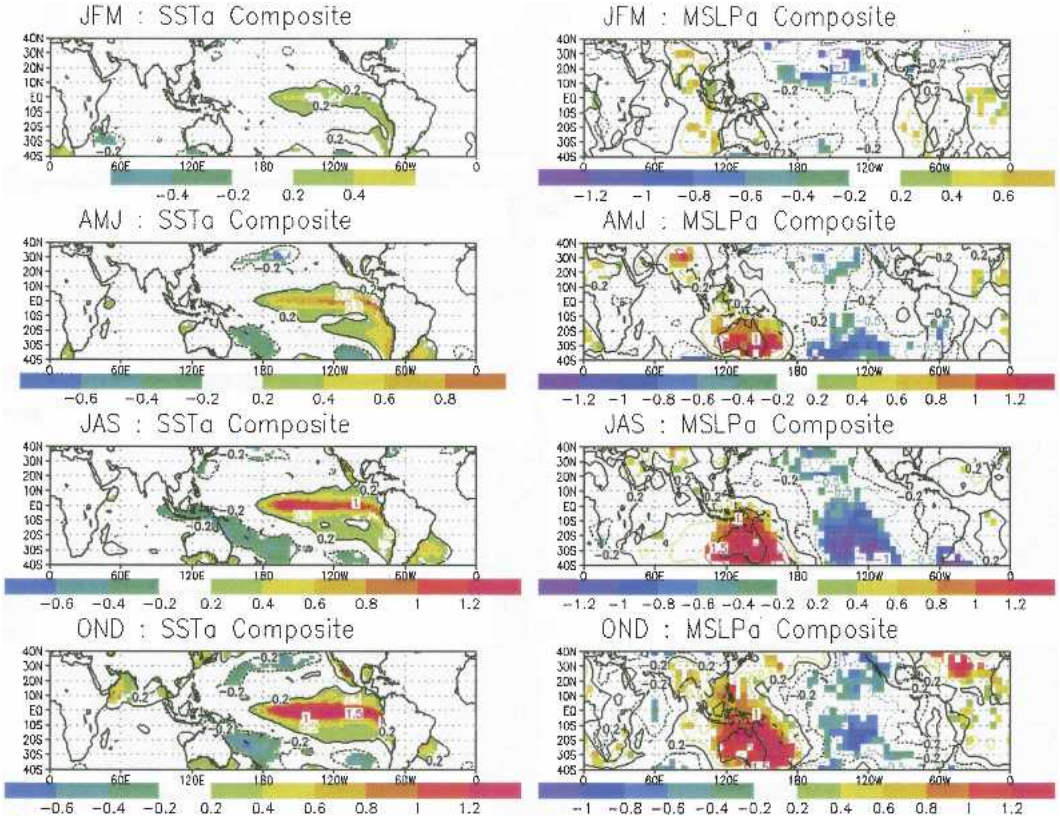

FIG. 4. (*Continued*)

central tropical Pacific. Significantly cooler than normal water also developed early near the east coast of Australia and intensified throughout the season. The line of separation between the warm and cool pools represents the position of the south Pacific convergence zone (SPCZ; Folland et al. 2002), which is more obvious in FP3 than either of the other two groups. The associated MSLP anomalies (Fig. 4c) depicted a clear pressure dipole with HP anomalies widespread and centered over eastern Australia and LP anomalies centered in the central Pacific as early as AMJ. The extremes of this pressure dipole were most proximal for this group and had the most southerly centers of action. These features likely explain the widespread effect on wheat yield throughout the continent in years associated with this FP.

The evolution of the EN events associated with years in each of the wheat FPs showed differences related to timing of onset and locations of the major SST and MSLP anomalies. The pressure anomalies associated with the three FPs shifted southward, and centers of action of dipoles became more proximal from FP1 to FP2 and FP3. These attributes likely influence the latitude of the subtropical ridge, which has significant association with rainfall variability in eastern Australia (Pittock 1975). Furthermore, the shift in tilt of the line of separation between warm and cool SST pools from years in FP1 and FP2 to those in FP3 suggests linkage to the location of the SPCZ (Folland et al. 2002), which has significant association with decadal variability in rainfall (Meinke et al. 2005). Decadal rainfall variability is known to have significant effects on rainfall and crop yields in Australia (Power et al. 1999). The SST anomaly patterns for years in FP3 had features similar to known decadal patterns (Allan 2000). The association was confirmed when we examined average decadal (9–13 yr) annual EOF component scores (Allan 2000) associated with years in each FP. Average values for years in FP1 and FP2 were close to zero, while years in FP3 had an average of 0.8.

This is the first analysis, to our knowledge, that identifies the most significant physical features associated with the evolution of EN events that could explain variability in their impact. The associations suggest that variability in impact is most likely forced by differences in the temporal evolution and spatial extent of the ocean–atmosphere patterns. Features outside the tropical Pacific are also contributing, as also found by Drosdowsky and Chambers (2001). Although we used Australian wheat yields as a bioindicator to elucidate variations in EN impacts, the insights gained from this study are potentially globally significant. The primary use of an integrative biological indicator has generated insight not uncovered to date by traditional climate analyses.

The results suggest climate system drivers responsible for variation in EN events and decadal rainfall patterns. However, predictability of such drivers may be limited as a result of the internal chaotic dynamics of the atmosphere or of the ENSO system itself (Cobb et al. 2003). The variability among years making up the average anomaly composites may reflect this. However, it would be useful to examine the potential climate system drivers using the increasing capabilities of general circulation models (Goddard et al. 2001). Any consequent improvement in discrimination among putative types of EN would be extremely valuable because spatial variation in impacts may become better predicted.

4. Conclusions

The analysis of relationships between shire wheat yields, shire rainfall, and global SSTs and MSLPs suggested three putative types of EN within the 24 EN events since the beginning of the last century. Three spatial modes of wheat yield variability were identified within the EN years. The first mode affected the northeastern region of Australia, the second mode the southern and northeastern regions, and the third mode the entire wheat-cropping region of Australia. Associated rainfall anomalies (during May–October) aligned very strongly in magnitude and spatial coherence with the yield footprints, which suggested a relatively strong connection to the persistent weather patterns caused by the ocean–atmosphere dynamics. The associated ocean–atmosphere dynamics differed in timing of onset and location of major ocean temperature and atmospheric pressure anomalies among the three groups. The analysis highlighted the importance of both a whole-Pacific basin (or near global) approach and the temporal dynamics of ENSO in relation to ENSO impact forecasting. The use of wheat as an integrative biological quantity in deriving broad spatial climatic patterns demonstrates its suitability as an additional diagnostic tool in determining plausible climatic mechanisms. The causal mechanisms for these putative EN types need to be investigated further using the increasing capabilities of general circulation models.

Acknowledgments. I want to thank Al Doherty for his programming support in generating the shire time series for wheat yield and rainfall.

REFERENCES

ABARE, 2002: Australian commodities. Australian Bureau of Agricultural and Resource Economics, Vol. 9, No. 3, Canberra, Australia, 113 pp.

Allan, R. J., 2000: ENSO and climatic variability in the last 150 years. *El Niño and the Southern Oscillation: Multiscale Variability and Its Impacts on Natural Ecosystems and Society,* H. F. Diaz and V. Markgraf, Eds., Cambridge University Press, 3–55.

——, J. A. Lindesay, and D. E. Parker, 1996: *El Niño Southern Oscillation and Climate Variability*. CSIRO Publishing, 405 pp.

Anderson, J. R., 1979: Impacts of climate variability in Australian agriculture: A review. *Rev. Market. Agric. Econ.,* **49,** 147–177.

Cane, M., 2000: Understanding and predicting the world's climate system. *Applications of Seasonal Climate Forecasting in Agricultural and Natural Ecosystems—The Australian Experience,* G. L. Hammer, N. Nicholls, and C. Mitchell, Eds., Kluwer Academic, 29–50.

Cobb, K. M., C. D. Charles, H. Cheng, and R. Lawrence Edwards, 2003: El Niño/Southern Oscillation and tropical Pacific climate during the last millennium. *Nature,* **424,** 271–276.

Drosdowsky, W., and L. E. Chambers, 2001: Near-global sea surface temperature anomalies as predictors of Australian seasonal rainfall. *J. Climate,* **14,** 1677–1687.

Folland, C. K., J. A. Renwick, M. J. Salinger, and A. B. Mullan, 2002: Relative influences of the Interdecadal Pacific Oscillation and ENSO on the South Pacific Convergence Zone. *Geophys. Res. Lett.,* **29,** 1643, doi:10.1029/2001GL014201.

Garnett, E. R., and M. L. Khandekar, 1992: The impact of large scale atmospheric circulations and anomalies on Indian monsoon droughts and floods and on world grain yields—A statistical analysis. *Agric. For. Meteor.,* **61,** 113–128.

Goddard, L., S. J. Mason, S. E. Zebiak, C. F. Ropelewski, R. Basher, and M. A. Cane, 2001: Current approaches to seasonal to interannual climate predictions. *Int. J. Climatol.,* **21,** 1111–1152.

Gong, X., and M. B. Richman, 1995: On the application of cluster analysis to growing season precipitation data in North America east of the Rockies. *J. Climate,* **8,** 897–931.

Hill, H. S. J., and Coauthors, 2001: Effects of seasonal climate variability and the use of climate forecasts on wheat supply in the U.S., Australia, and Canada. *Impact of El Niño and Climatic Variability on Agriculture*, C. Rosenzweig et al., Eds., American Society of Agronomy Special Publ. 63, 101–123.

Hogan, L., K. Woffendon, K. Honslow, and S. Zeng, 1995: The impact of the 1994–1995 drought on the Australian economy. *Proc. Australian Institute of Agricultural Science 1995 Drought Forum*, ABARE Conf. Paper 95.10, Warwick Farm, New South Whales, Australia, ABARE, 21–33.

Kaiser, H. F., 1958: The varimax criterion for analytic rotation in factor analysis. *Psychometricka,* **23,** 187–200.

Mason, S. J., and L. Goddard, 2001: Probabilistic precipitation anomalies associated with ENSO. *Bull. Amer. Meteor. Soc.,* **82,** 619–638.

McBride, J. L., and N. Nicholls, 1983: Seasonal relationships between Australian rainfall and the Southern Oscillation. *Mon. Wea. Rev.,* **111,** 1998–2004.

Meinke, H., W. Wright, P. Hayman, and D. Stephens, 2003: Managing cropping systems in variable climates. *Principles of Field Crop Production*, 4th ed. J. Pratley, Ed., Oxford University Press, 26–77.

——, P. deVoil, G. L. Hammer, S. Power, R. Allan, R. C. Stone, C. Folland, and A. Potgieter, 2005: Rainfall variability at decadal and longer time scales: Signal or noise? *J. Climate,* **18,** 89–96.

Mimmack, G. M., S. J. Mason, and S. G. Galpin, 2001: Choice of distance matrices in cluster analysis: Defining regions. *J. Climate,* **14,** 2790–2797.

Nelson, R. A., D. P. Holzworth, G. L. Hammer, and P. T. Hayman, 2002: Infusing the use of seasonal climate forecasting into crop management practice in North East Australia using discussion support tools. *Agric. Syst.,* **74,** 393–414.

Nicholls, N., 1985: Impact of the Southern Oscillation on Australian crops. *J. Climatol.,* **5,** 553–560.

Nix, H. A., 1975: The Australian climate and its effects on grain yield and quality. *Australian Field Crops, Wheat and Other Temperate Cereals,* A. Lazenby and E. M. Matheson, Eds., Vol. 1, Angus and Robertson, 83–226.

Pittock, A. B., 1975: Climatic change and the patterns of variation in Australian rainfall. *Search,* **6** (11–12), 498–504.

Potgieter, A. B., G. L. Hammer, and D. Butler, 2002: Spatial and temporal patterns in Australian wheat yield and their relationship with ENSO. *Aust. J. Agric. Res.,* **53,** 77–89.

Power, S. B., T. Casey, C. Folland, A. Colman, and V. Mehta, 1999: Inter-decadal modulation of the impact of ENSO on Australia. *Climate Dyn.,* **15,** 319–324.

Rimmington, G. M., and N. Nicholls, 1993: Forecasting wheat yields in Australia with the Southern Oscillation Index. *Aust. J. Agric. Res.,* **44,** 625–632.

Ropelewski, C. F., and M. S. Halpert, 1987: Global and regional scale precipitation patterns associated with the El Niño/Southern Oscillation. *Mon. Wea. Rev.,* **115,** 1606–1626.

——, and P. D. Jones, 1987: An extension of the Tahiti–Darwin Southern Oscillation index. *Mon. Wea. Rev.,* **115,** 2161–2165.

Smith, T. M., and R. W. Reynolds, 2003: Extended reconstruction of global sea surface temperatures based on COADS data (1854–1997). *J. Climate,* **16,** 1495–1510.

Stephens, D. J., 1998: Objective criteria for estimating the severity of drought in the wheat cropping areas of Australia. *Agric. Syst.,* **59,** 315–332.

——, and T. J. Lyons, 1998: Rainfall-yield relationships across the Australian wheatbelt. *Aust. J. Agric. Res.,* **49,** 211–223.

——, D. G. Butler, and G. L. Hammer, 2000: Using seasonal climate forecasts in forecasting the Australian wheat crop. *Applications of Seasonal Climate Forecasting in Agricultural and Natural Ecosystems—The Australian Experience,* G. L. Hammer, N. Nicholls, and C. Mitchell, Eds., Kluwer Academic, 351–366.

Stone, R. C., G. L. Hammer, and T. Marcussen, 1996: Prediction of global rainfall probabilities using phases of the Southern Oscillation Index. *Nature,* **384,** 252–255.

Trenberth, K. E., 1997: The definition of El Niño. *Bull. Amer. Meteor. Soc.,* **78,** 2771–2777.

Troup, A. J., 1965: The Southern Oscillation. *Quart. J. Roy. Meteor. Soc.,* **91,** 490–506.

White, B., 2000: The importance of climate variability and seasonal forecasting to the Australian economy. *Applications of Seasonal Climate Forecasting in Agricultural and Natural Ecosystems—The Australian Experience,* G. L. Hammer, N. Nicholls, and C. Mitchell, Eds., Kluwer Academic, 1–22.